21st Annual International Conference on Mechanical Engineering-ISME2013
7-9 May, 2013, School of Mechanical Eng., K.N.Toosi University, Tehran, Iran

ISME2013-1912

Fundamental asymmetric lamb wave (a_0) interaction with a rectangular notch in a plate using Elastodynamic Finite Integration Technique (EFIT)

Hussein Rappel[1], Aghil Yousefi-Koma[2]

[1] Graduate student, Advanced Dynamic and Control Systems Laboratory (ADCSL), School of Mechanical Engineering, College of Engineering, University of Tehran, Tehran, Iran.
[2] Professor, Advanced Dynamic and Control Systems Laboratory (ADCSL), School of Mechanical Engineering, College of Engineering, University of Tehran, Tehran, Iran; Email: aykoma@ut.ac.ir.

Abstract
Fundamental asymmetric lamb wave's interactions with rectangular notches in a steel plate are investigated in this paper. Elastodynamic finite integration technique previously mainly used to study wave propagation in elastic media is adopted to study lamb wave interaction with defects. Simulation examples are presented to illustrate the reflection and transmission coefficients' variations with defect's height, for both symmetric and asymmetric modes. Results show as the depth of notch increases reflection coefficients for both symmetric mode and asymmetric mode increase. However, when the depth of notch increases transmission coefficient for asymmetric mode decreases which means the main part of transmitted energy is carried by symmetric mode generated when the fundamental asymmetric mode interacts with defect. This simulation could be a valuable tool for the research of lamb wave's applications in nondestructive testing (NDT) field, as the problem of lamb wave interaction with discontinuities can be used to study defect sizing problem.

Keywords: EFIT, Lamb waves, Wave scattering, Defect sizing

Introduction

Lamb wave testing technique is increasingly used for assessing defects in thin-wall structures like plate and pipes [1-3]. Lamb waves are waves whose wave length is the same order as thickness of structure [4]. The main advantage of lamb wave technique is that they allow long-range inspection in contrast to traditional ultrasonic testing where the coverage is limited to a small area in vicinity of each transducer. Lamb waves were first described theoretically by Horace lamb in 1917 [5]. These waves arise from coupling between shear and longitudinal waves reflected at the top and bottom edges of thin-wall structure. Lamb wave theory can be found in a number of text books [6]. Defects such as corrosion fatigue cracks cause changes in effective thickness and local material properties and therefore measurement of variations in lamb wave can be used to assessing integrity of structure [1].

Successful use of lamb wave technique as an inspection system requires the understanding of the schemes of its propagation in thin-wall structure and its scattering at defect. Many researchers have tried to study interaction of lamb wave with a single defect like crack, notch and circular cavity using various methods e.g. Grahn (2003) used analytical solution to study lamb wave to study scattering from a circular [7]. Alleyne and Cawley (1992) studied the interaction of lamb wave with notches of different size and angle with respect to normal of the plate surface by using time-domain FEM combined with 2D- Fourier transform [8], Lowe et al. (2002) used finite element time-domain simulations to analyze the interaction of fundamental symmetric and asymmetric modes with surface braking rectangular notches [9, 10]; Bennmedour et al. (2008) used FEM to study the fundamental lamb modes interaction with symmetrical and asymmetrical discontinuities [11, 12]. Lovstad and cawely (2012) used finite element method to study reflection of fundamental torsional mode from multiple circular holes and pit cluster in pipes they also evaluated their simulation results with experimental results [13]. Cho and Rose et al. (2000) applied the hybrid boundary element method (BEM) along with mode expansion technique to study interaction of lamb wave with half elliptical surface braking defects [14]. Shen et al. (2011) applied the same method to examine lamb wave interactions with transverse defects in elastic plates [15].

In this work elastodynamic finite integration technique is used to study fundamental asymmetric mode interaction with notches of different sizes in a steel plate. Historically Finite integration technique was introduced by Weiland in electrodynamics. Fellinger and Langenberg used Weiland's idea to governing equations of ultrasonic waves in solid calling it EFIT [16]. EFIT is a grid based numerical time-domain method using velocity-stress formalism, and easily treats with different boundary conditions which are essential to model ultrasonic wave propagation [17]. Because of its relative simplicity and flexibility, Schubert et al used EFIT equations to cylindrical coordinates (CEFIT) to simulate asymmetric wave propagation in pipes with a 2D grid [18]. Schubert also used Finite Integration Technique to simulate elastic wave propagation in porous concrete and showed efficiency of EFIT to model a diverse range of applications [19].

To study the interaction of fundamental asymmetric mode with notches, reflection and transmission

coefficients are calculated using the time-domain signals obtained by EFIT. Simulations are done on 2D a steel plate with rectangular notches of varying depth. Results show as the depth of notch increases reflection coefficient for both symmetric and asymmetric mode will increase.

Calculation of transmission coefficients show, for notch with greater depths transmission coefficient for asymmetric mode decreases, however symmetric mode it will increase which means as the depth of notch increases, main part of transmitted energy is conveyed by converted mode (symmetric).

The Elastodynamic Finite Integration Technique for Linear Elastics

Governing Equations

The governing equations of elastic waves in a general media are Cauchy equation of motion and equation of deformation rate. These equations are given in integral form for a finite volume V, with surface S:

$$\frac{\partial}{\partial t}\int_V \rho v_i\, dV = \int_S T_{ij} n_i\, dS + \int_V f_i\, dV \tag{1}$$

$$\frac{\partial}{\partial t}\int_V s_{ijkl} T_{kl}\, dV = \frac{1}{2}\int_S \left(v_i n_j + v_j n_i\right) dS \tag{2}$$

Where v is the particle velocity vector, T is stress tensor, ρ is density, n is the outward normal vector on surface S, f is the body force vector and s is the compliance tensor. The inverse of s is the stiffness tensor c. Thus using stiffness tensor deformation rate equation can be expressed in other form.

$$\frac{\partial}{\partial t}\int_V T_{kl}\, dV = \frac{1}{2}\int_S c_{klij}\left(v_i n_j + v_j n_i\right) dS = \int_S c_{klij} v_i n_j\, dS \tag{3}$$

In the case of isotropic material c can be written as:

$$c_{ijkl} = \lambda\delta_{ij}\delta_{kl} + \mu\left(\delta_{ik}\delta_{jl} + \delta_{il}\delta_{jk}\right) \tag{4}$$

Where λ and μ are lame constants.

Spatial Discretized Form of Two Dimensional EFIT

Consider the Cartesian coordinate $\{x, y, z\}$ and ultrasonic wave which propagates in two dimensional xz - plane. To apply FIT to Equations 1 and 2 squares shown in Figure 1 are used as integral volume V assuming constant v and T for each volume. The final results for discretized form are

$$\frac{\partial v_x(x_0, z_0)}{\partial t} = \frac{1}{\rho}\left[\frac{T_{xx}\left(x_0+\frac{\Delta x}{2}, z_0\right) - T_{xx}\left(x_0-\frac{\Delta x}{2}, z_0\right)}{\Delta x} + \frac{T_{xz}\left(x_0, z_0+\frac{\Delta z}{2}\right) - T_{xz}\left(x_0, z_0-\frac{\Delta z}{2}\right)}{\Delta z} + \frac{f_x}{\Delta x \Delta z}\right] \tag{5}$$

A same manner of integration Equation 1 about an v_z integration cell centered at (x_1, z_1) results in

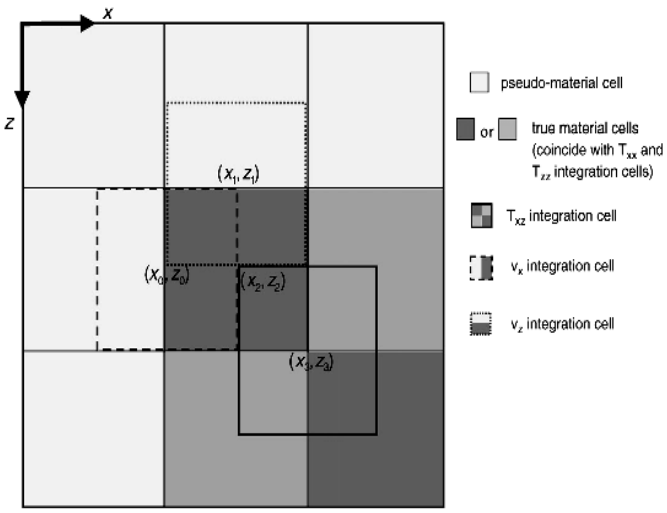

Figure 1: Definition of integration cells for stress and velocity components. The geometry consists of four true material cells and four pseudo-material cells [17].

$$\frac{\partial v_z(x_1, z_1)}{\partial t} = \frac{1}{\rho}\left[\frac{T_{xz}\left(x_1+\frac{\Delta x}{2}, z_1\right) - T_{xz}\left(x_1-\frac{\Delta x}{2}, z_1\right)}{\Delta x} + \frac{T_{zz}\left(x_1, z_1+\frac{\Delta z}{2}\right) - T_{zz}\left(x_1, z_1-\frac{\Delta z}{2}\right)}{\Delta z} + \frac{f_z}{\Delta x \Delta z}\right] \tag{6}$$

Now using the normal stress equations, integration of Equation 3 about T_{xx} and T_{zz} centered at (x_2, z_2) yields

$$\frac{\partial T_{xx}(x_2, z_2)}{\partial t} = (\lambda+2\mu)\left[\frac{v_x\left(x_2+\frac{\Delta x}{2}, z_2\right) - v_x\left(x_2-\frac{\Delta x}{2}, z_2\right)}{\Delta x}\right] + \lambda\left[\frac{v_z\left(x_2, z_2+\frac{\Delta z}{2}\right) - v_z\left(x_2, z_2-\frac{\Delta z}{2}\right)}{\Delta z}\right] \tag{7}$$

$$\frac{\partial T_{zz}(x_2, z_2)}{\partial t} = (\lambda+2\mu)\left[\frac{v_z\left(x_2, z_2+\frac{\Delta z}{2}\right) - v_z\left(x_2, z_2-\frac{\Delta z}{2}\right)}{\Delta z}\right] + \lambda\left[\frac{v_x\left(x_2+\frac{\Delta x}{2}, z_2\right) - v_z\left(x_2-\frac{\Delta x}{2}, z_2\right)}{\Delta x}\right] \tag{8}$$

Finally integration of Equation 3 over T_{xz} integration cell centered at (x_3, z_3) the intersection for material cells results in

$$\frac{\partial T_{xz}(x_3, z_3)}{\partial t} = \mu\left[\frac{v_x\left(x_3, z_3+\frac{\Delta z}{2}\right) - v_x\left(x_3, z_3-\frac{\Delta z}{2}\right)}{\Delta z} + \frac{v_z\left(x_3+\frac{\Delta x}{2}, z_3\right) - v_z\left(x_3-\frac{\Delta x}{2}, z_3\right)}{\Delta x}\right] \tag{9}$$

As shown in Figure 1 to simplify indexing into stress and velocity arrays of staggered grids when programming the numerics and to keep the same array

sizes for all quantities pseudo-material cells are used. These cells have the same material properties as the true material they are added to but are not part of physical simulations.

Time Discretization

Central differences are used to discretize the equations in time domain which results in the velocity and stress components being staggered in time by $\frac{\Delta t}{2}$ [18].

$$v^n = v^{n-1} + \Delta t \dot{v}^{n-\frac{1}{2}} \quad (10)$$

$$T^{n+\frac{1}{2}} = T^{n-\frac{1}{2}} + \Delta t \dot{T}^n \quad (11)$$

Where Δt is time interval, superscript n is integer number of time step and dot $\{\bullet\}$ denotes the time differentiation.

Equations 5- 9 are solved at all points in simulation space and by use of Equations 10 and 11 the simulation proceeds in time in a 'leap frogging' manner. A specific stability condition and adequate spatial resolution must be satisfied to guarantee EFIT convergence and accurate answers [17, 18].

The model of the object

In this part, the interaction of fundamental asymmetric mode with notches of different sizes in a steel plate will be modeled. The investigation is done on a simple plane strain model with length $l = 400\ mm$ and the thickness $d = 2\ mm$, shown in Figure 2. The notch width is considered $0.4\ mm$ in all simulations.

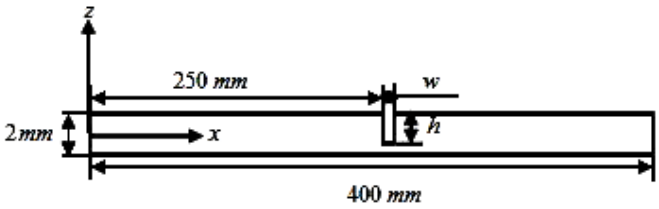

Figure 2: Schematic of model used for studying interaction lamb wave with a defect in a steel plate.

Table 1 shows material properties used in this paper.

Table 1: Material properties used for simulation

Property	Value
Density	7700 (kg/m^3)
Elastic Modulus	195Gpa
Lame constant λ	96.95Gpa
Lame constant μ	76.17Gpa

Correct selection of excitation signal mode and frequency range is essential for use of lamb wave technique in an inspection system. Since properties governing lamb wave propagation and interaction with defect are very complicated, excitation parameters should be chosen carefully. To excite fundamental asymmetric mode purely, excitation pattern shown in Figure 3 is used in this study.

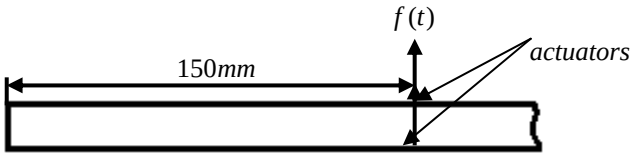

Figure 3: Fundamental asymmetric (a_0) mode excitation pattern

Excitation signal used in this paper is raised cosine pulse with five cycles and the center frequency of $f_c = 500kHz$ (Figure 4). Because of simulation accuracy and stability, the spatial mesh sizes in both x and z directions is set $2\mu m$ ($\Delta x = \Delta z = 2\mu m$) and time step is chosen $20\ ns$.

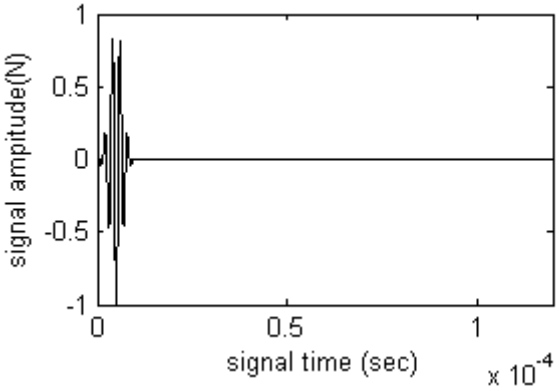

Figure 4: Excitation pulse with center frequency of $f_c = 500kHz$.

To study lamb wave interaction with the notches, points $x_{s1} = 200mm$ (at the left side of notch) and $x_{s2} = 300mm$ (at the right side of notch) are considered as sensors. Figure 5 represents time history of normal component of velocity (v_z) obtained by EFIT at the left sensor (s_1) for the plate with notch of $0.4\ mm$ width and $0.8\ mm$.

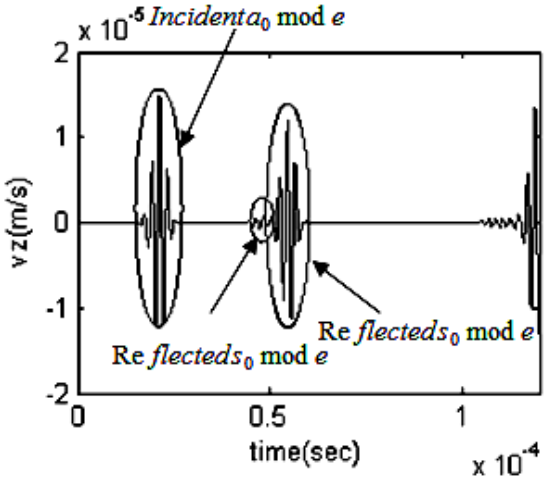

Figure 5: Time history of point $x_{s1} = 200mm$, for the plate with notch of $0.4\ mm$ width and $0.8\ mm$. Sensor output is the normal component of velocity (v_z).

As shown in Figure 5 since the actuator is placed far enough from the left edge, the reflection signal from

edge will not interfere with the reflection signals from notch.

Results and discussions

The reflection and transmission coefficients are calculated using time-domain signals generated by EFIT. Ratio of maximum amplitudes of reflected modes to incident mode at left sensor is used to calculate the reflection coefficients (Figure 6).

Figure 6 shows reflection coefficients as a function of notch's depth. As shown in the figure, both s_0 and a_0 reflection coefficients increase as the depth of notch increases; however for symmetric mode these coefficients are approximately constant. Also for asymmetric mode the slope of the graph decreases as the depth of defect increases.

Repeating the same procedure for sensor at $x_{s2} = 300mm$ transmission coefficients are obtained for both symmetric and asymmetric modes (Figure 7).

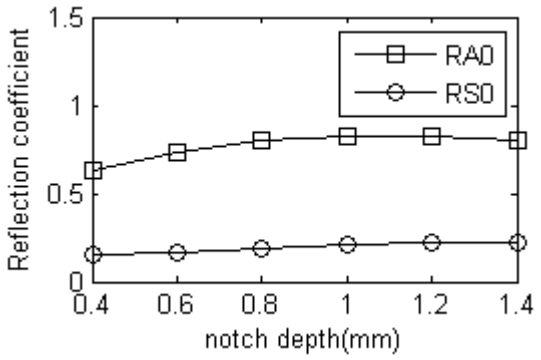

Figure 6: Reflection coefficients for symmetric and asymmetric modes, $f = 500kHz$ a_0 incident mode, rectangular notch.

Numerical results show, transmission coefficient for symmetric mode increases as the depth of notch grows, however w the depth equals 1.2 mm transmission ratio reaches to its maximum and after that point decreases. In contrast to symmetric mode for asymmetric mode transmission coefficient decreases as the depth of notch grows, nevertheless when the depth reaches to 1mm transmission coefficient starts to increase.

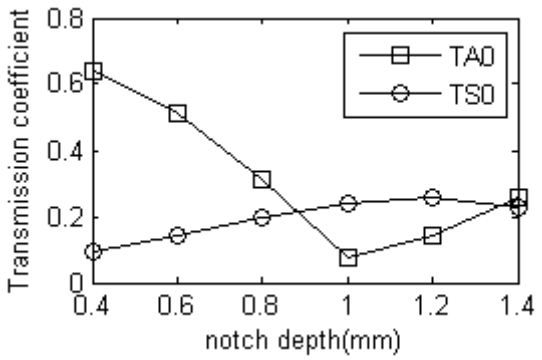

Figure 7: Transmission coefficients for symmetric and asymmetric modes, $f = 500kHz$ a_0 incident mode, rectangular notch.

Also Figure 7 shows, when the depth of notch is greater than 0.8 mm transmission coefficient for asymmetric mode is less than transmission coefficient for symmetric mode, which means as the depth of notch increases most of transmitted energy in conveyed by converted mode and most of reflected energy is conveyed by incident mode.

Conclusions

A two-dimensional EFIT code was developed to calculate transmission and reflection coefficients of lamb wave on a plate with rectangular notch. Results presented in this paper can be used for sizing investigation of defects. Simulation results showed reflection coefficients increase for both a_0 and s_0 modes. However, changes in symmetric mode's reflection coefficient are small in comparison to asymmetric mode. Furthermore, results showed when the depth of the notch grows most of transmitted energy is conveyed by converted mode (symmetric), and incident mode (asymmetric) containing main part of the reflected energy.

Calculations in this paper were conducted on a ordinary PC (Core i5, 2.4GHz, 4GB RAM). Each simulation took about 13 minutes to complete.

References

[1] Yu, J, G., Ratolojanhary, F, E., Lebvre, and J, E., 2011. "Guided waves in functionally graded viscoelastic plates". *Journal of Composite Structures*, 93(11), June, pp. 2671-2677.

[2] Raghavan, A., and Cesnik, C, E, S., 2007. "Review of guided wave structural health monitoring". *Journal of The Shock and Vibration Digest*, 39(2), March, pp. 91-113.

[3] Rathod, V, T., and Mahapatra, D, R., 2011. "Ultrasonic lamb wave based monitoring of corrosion type of damage in plate using a circular array of piezoelectric transducer". *Journal of NDT&E International*, 44(7), November, pp. 628-636.

[4] Yeum, C, M., Sohn, H., and Ihn, J, B., 2011. "Lamb wave mode decomposition using concentric ring and circular piezoelectric transducer". *Journal of Wave Motion*, 48 (4), June, pp. 358-370.

[5] Sorohan, S., Constantin, N., Gavan, and M., Anghel, V., 2011. "Extraction of dispersion curves for waves propagating in free complex waveguides by standard finite element codes". *Journal of Ultrasonics*, 51(4), May, pp. 503-515.

[6] Graff, K, F., 1991. *Wave motion on elastic solids*. Dover Publications, New York.

[7] Grahn, T., 2003. "Lamb wav scattering from a circular partly through-thickness hole on plate". *Journal of Wave Motion*, 37(1), January, pp. 63-80.

[8] Alleyne, D, N., and Cawley, P., 1992. "The interaction of lamb wave with defects". *Journal of Transactions on Ultrasonics*,

Ferroelectrics, and Frequency Control, 39(3), May, pp. 381-397.

[9] Lowe, M, J, S., and Diligent, O., 2002. "Low-frequency reflection characteristics of S_0 lamb wave from a rectangular notch in plate". *Journal of Acoustical Society of America*, 111(1), October, pp. 64-74.

[10] Lowe, M, J, S., and Diligent, O., 2002. "Low-frequency reflection characteristics of A_0 lamb wave from a rectangular notch in plate". *Journal of Acoustical Society of America*, 112(6), December, pp. 2612-2622.

[11] Benmeddour, F., Grondel, S., Assaad, J., and Moulin, E., 2008. "Study of the fundamental lamb modes interaction with symmetrical notches". *Journal of NDT&E international*, 41(1), January, pp. 1-9.

[12] Benmeddour, F., Grondel, S., Assaad, J., and Moulin, E., 2008. "Study of the fundamental lamb modes interaction with asymmetrical discontinuities". *Journal of NDT&E international*, 41(5), July, pp. 330-340.

[13] Lovstad, A., and Cawley, P., 2012. "The reflection of the fundamental torsional mode from pit clusters in pipes". *Journal of NDT&E international*, 46, March, pp. 83-93.

[14] Cho, Y., and Rose, J, L., 2000. "An elastodynamic hybrid boundary element study for elastic guided wave interactions with a surface braking defect". *International Journal of SOLIDS and STRUCTURES*, 37, October, pp. 4103-4124.

[15] Shen, W., Songling, H., and Wei, Z., 2011. "Simulation of lamb wave's interaction with transverse internal defects in an elastic plate". *Journal of Ultrasonics*, 51(4), May, pp.432-440.

[16] Marklein, R., 2002. *The finite integration technique as a general tool to compute acoustic, electromagnetic, elastodynamic, and coupled wave fields, in: W. Stone (Ed.), Review of Radio Science: 1999–2002 URSI*. IEEE Press and John Wiley and Sons, New York.

[17] Calvo, D, C., Rudd, K, E., Zampolli, M., Sanders, W, M., Bibee, and L, D., 2010. "Simulation of acoustic scattering from an aluminum cylinder near a rough interface using the elastodynamic finite integration technique". *Journal of Wave Motion*, 47(8), December, pp.616-634.

[18] Schubert, F., Peiffer, A., Kohler, B., and Sanderson, T., 1998. "The elastodynamic finite integration technique for waves in cylindrical geometries". *Journal of Acoustical Society of America*, 104 (5), July , pp.2604-2614.

[19] Schubert, F., and Koehler, B., 2001. "Three-dimensional time domain modeling of ultrasonic wave propagation in concrete in explicit consideration of aggregates and porosity". *Journal of Computational Acoustics*, 9(4), December, pp. 1543-1560.